Geochimica et Cosmochimica Acta, Vol. 69, No. 12, pp. 3017–3027, 2005

0016-7037/05 $30.00 + .00

doi:10.1016/j.gca.2004.12.019

Nanoscale effects of strontium on calcite growth: An in situ AFM study in the absence of vital effects

LAURA E. WASYLENKI,[1,†] PATRICIA M. DOVE,[1,*] DARREN S. WILSON,[1] and JAMES J. DE YOREO[2]

[1]Department of Geosciences, Virginia Polytechnic Institute and State University, Blacksburg, Virginia 24061, USA
[2]Department of Chemistry and Materials Science, Lawrence Livermore National Laboratory, Livermore, California 94551, USA

(*Received June* 1, 2004; *accepted in revised form December* 13, 2004)

Abstract—This experimental study presents in situ measurements of step migration rates for layer growth of calcite at various levels of superaturation and fluid Sr concentrations. Our results show that Sr has complex behavior as an impurity. At low concentrations, Sr promotes faster growth. This effect may be associated with slight shifts in calcite solubility when Sr is incorporated or may be due to as yet uncharacterized kinetic effects. At higher concentrations, Sr stops step advancement by pinning kink-sites or step edges. The threshold concentration of Sr needed to halt growth is positively correlated with supersaturation.

Addition of Sr to the calcite growth system leads to significant changes in hillock morphology. Hillocks become elongate perpendicular to the projection of the *c*-glide plane, in contrast to the changes previously reported for Mg. Step edges also become scalloped, and the boundary between the obtuse-stepped flanks disappears and is replaced by a new step direction with edges parallel to [010].

Incorporation of Sr was measured at two supersaturation levels and identical fluid [Sr]. The results indicate a strong positive correlation between fluid supersaturation and crystal Sr content. Further, Sr is strongly fractionated between obtuse- and acute-stepped flanks by a factor of approximately two. The sensitivity of Sr uptake to supersaturation may explain apparently contradictory results in the literature regarding whether Sr uptake in the calcite produced by one-celled marine organisms is controlled by temperature. In addition, Sr contents of natural calcite samples may be good indicators of the levels of supersaturation at which the crystals grew.

Results of this investigation demonstrate the importance of understanding impurity-specific interactions with calcite growth surfaces at the microscopic scale. Despite similar chemical behavior in some systems, Mg and Sr clearly have very different effects on calcite growth. If Sr and other impurities are to be used as robust indicators of growth conditions in natural calcite samples, well grounded understanding of the mechanisms of recording trace element signatures in calcite is an essential step toward correctly deciphering paleoenvironmental signals from fossil calcite compositions. *Copyright © 2005 Elsevier Ltd*

1. INTRODUCTION

The potential for extracting robust, paleoenvironmental information from the compositional signatures recorded in biogenic carbonates has garnered much attention from earth scientists. For several decades paleoclimatologists have attempted to infer ancient climatic conditions by interpreting chemical signals in ice and rock samples. Recently, the concentrations of specific trace impurities in calcite and aragonite precipitated by modern marine organisms or found in core-top sediments have been shown to correlate with various parameters of the growth environment, including temperature, salinity, nutrient levels, carbonate concentration, and water chemistry (see Lea, 1999, for a helpful review). These findings suggest that elemental paleoproxies in calcite and aragonite have the potential to become powerful tools in reconstruction of the past from the fossil record. For this potential to be realized, it is essential that the physical and chemical mechanisms underlying the chemical proxies be discovered and rigorously investigated. Without fundamental understanding, such proxies rely upon empirical correlations and must be applied to natural sample suites with caution.

Among the trace constituents of calcite with great promise is strontium. Second only to magnesium in abundance as a cationic impurity, Sr^{2+} substitutes for Ca^{2+} in the calcite crystal lattice (Pingitore et al., 1992). Despite the conservative behavior of Sr^{2+} in seawater, significant variations in Sr content have been documented for natural and laboratory-grown biogenic (Cronblad and Malmgren, 1981; Delaney et al., 1985; Elderfield et al., 1996; Rosenthal et al., 1997; Lea et al., 1999; Purton et al., 1999; Stoll et al., 2002) and inorganic calcite crystals (Holland et al., 1964; Katz et al., 1972; Lorens, 1981; Graham et al., 1982; Mucci and Morse, 1983; Paquette and Reeder, 1995; Tesoriero and Pankow, 1996; Martin et al., 1997).

Studies of the dependence of Sr concentration on various physical and chemical parameters are numerous, but the results taken as a whole are difficult to interpret. For example, published studies of cultured, biogenic calcite disagree on the extent to which temperature influences Sr behavior (Cronblad and Malmgren, 1981; Delaney et al., 1985; Rosenthal et al., 1997; Lea et al., 1999; Stoll et al., 2002). Other investigations of biogenic samples suggest that pressure, precipitation rate, salinity, pH, solution Sr concentration, and/or metabolic factors may play roles in governing interactions between Sr and calcite (Graham et al., 1982; Carpenter and Lohmann, 1992; Elderfield et al., 1996; Rosenthal et al., 1997; Lea et al., 1999; Purton et al., 1999; Rickaby et al., 2002; Stoll et al., 2002).

* Author to whom correspondence should be addressed (dove@vt.edu).
† *Present address:* Department of Geological Sciences, Arizona State University, Tempe, Arizona 85287, USA.

Experimental investigations of inorganic calcite growth in the presence of Sr have mostly involved bulk powder samples, using highly supersaturated solutions (Katz et al., 1972; Lorens, 1981; Mucci and Morse, 1983; Tesoriero and Pankow, 1996). In these circumstances growth occurs far from equilibrium, and only bulk properties of solutions and solids can be measured. The crystal growth mechanism is unobserved and unknown, but may well be dominated by two-dimensional heterogeneous or homogeneous nucleation, because reaction rates are very fast (Teng et al., 2000). Taken together, the complicated and sometimes contradictory results of these studies underscore the need for better knowledge of how impurities such as Sr act upon and are acted upon by growing calcite crystals.

In another type of experiment described by Paquette and Reeder (1995), a polygonal growth hillock, representing near-equilibrium growth, was precipitated toward the end of a free-drift experiment (Gruzensky, 1967) that began with strongly supersaturated solution containing multiple impurities. Sr concentrations were found to differ substantially between hillock flanks with geometrically distinct monomolecular step types, indicating that interactions between Sr cations and growth surfaces are affected by the configurations of bonding sites available at the mineral surface. This result further emphasizes the importance of looking beyond bulk properties to understand phenomena taking place at the mineral-solution interface.

Paleoproxies can be applied and interpreted robustly and to full advantage only when grounded by thorough knowledge of how they work. While previous studies have contributed much to what we know about calcite in the presence of Sr, a new approach is required to identify and quantify the mechanisms underlying proxy relationships between Sr and physical and chemical conditions of growth, including not only externally imposed parameters such as supersaturation, fluid Sr content, and temperature but also the details of surface morphology such as the orientation and density of atomic steps. In short, this new approach must involve direct observation and quantitative measurement of thermodynamic and kinetic controls on Sr behavior at the nanometer scale.

To understand completely the controls on Sr in natural samples from the bottom up is a daunting challenge, but in recent years, developments in nanoscale imaging and elemental analysis have made this increasingly feasible. Here we present in situ atomic force microscopy (AFM) measurements of calcite growth kinetics in the presence of Sr. Using this method, we observed the near-equilibrium growth of polygonal hillocks and quantified step migration rates as a function of solution supersaturation and Sr concentration. This study was conducted in the inorganic system to establish thermodynamic and kinetic effects in the absence of biologic, or "vital," effects. Once the inorganic system is understood, biologic complexities can be deconvolved more easily from the patterns observed in natural calcite samples. We find that, despite chemical similarities, Mg^{2+} and Sr^{2+} have strikingly different interactions with calcite surfaces during growth. Whereas Mg^{2+} inhibits growth through incorporation (Davis et al., 2000; Davis et al., 2004; Wasylenki et al., in press), Sr^{2+} can either inhibit or enhance growth, depending on its concentration in solution relative to degree of supersaturation. To our knowledge, this is the first case of an impurity causing accelerated and continuous growth relative to the nominally impurity-free system to be observed and documented at the nanoscale. Astilleros et al. (2003) reported faster propagation of a single, monomolecular step of calcite in the presence of Sr, but growth ceased with the next step.

We also present quantitative measurement of Sr contents in calcite grown at conditions documented by our AFM work. Precise information about the extent and spatial distribution of Sr in calcite has been coupled with direct observation of growth mechanism and kinetics for the first time. We report segregation coefficients for Sr at the conditions of these experiments. Note that we deliberately avoid the term "partition coefficient," which applies to systems at thermodynamic equilibrium. Because the incorporation of impurities in crystals growing from aqueous solutions typically depends dramatically on step geometry, kinetic factors associated with step-impurity interactions clearly play an important, if not dominant, role in determining incorporation (Watson, 1996; Smolsky et al., 1999; Kahr and Gurney, 2001; De Yoreo et al., 2002; Watson, 2004). Segregation coefficients, on the other hand, simply quantify the distribution of impurities between crystal and solution during steady-state growth, even in this kinetically controlled regime. Our results below indeed indicate a strong correlation between Sr incorporation and degree of supersaturation.

2. EXPERIMENTAL AND ANALYTICAL METHODS

2.1. Preparation of Growth Solutions

Solutions supersaturated with respect to calcite were prepared from high-purity $NaHCO_3$, $CaCl_2 \cdot 2H_2O$, NaCl, and $SrCl_2 \cdot 6H_2O$ dissolved in distilled deionized (18 MΩ) water. These reagent stock solutions were pipetted in appropriate proportions to make 100 mL batches of the desired growth recipes as needed. Several microliters of 1 M NaOH were added to each solution to achieve a pH near 8.5 before the solution was loaded into a syringe and pumped into the sample chamber. All solutions contained 0.1 molal NaCl as background electrolyte.

The concentrations of $NaHCO_3$ and $CaCl_2$ are varied to make solutions over a range of degrees of supersaturation. In this paper, calcite supersaturation (σ) is expressed as:

$$\sigma = \ln\left(\frac{a_{Ca^{2+}} a_{CO_3^{2-}}}{K_{sp}}\right) \quad (1)$$

where $a_{Ca^{2+}}$ and $a_{CO_3^{2-}}$ are the activities of the Ca^{2+} and CO_3^{2-} ions, and K_{sp} is the solubility product of pure calcite. Solutions used in this study have σ values of 0.55, 0.67, 0.76, 0.93, and 1.17. $SrCl_2$ concentrations ranged from 0 to 3×10^{-4} molal. Although substantially higher than found in seawater, these concentrations were chosen to avoid spontaneous nucleation of strontianite and to cover the range over which the effects of Sr could be seen clearly. All solution compositions used in this study are listed in Table 1.

The recipes for growth solutions were determined using the computer software package, The Geochemist's Workbench, with the assumption of a closed system with respect to CO_2. Solubility constants for calcite and related species were computed from the equations of Plummer and Busenberg (1982) and inserted into the program database. To uniquely constrain the recipes, pH was fixed at 8.5, and the ratio $a_{Ca^{2+}}/a_{CO_3^{2-}}$ was fixed at 1.0. Input concentrations of $NaHCO_3$ and $CaCl_2$ were varied iteratively until solutions with the desired degrees of calcite supersaturation were found. Values of σ are given only for the pure system and have not been corrected for addition of $SrCl_2$; according to The Geochemist's Workbench, the effect on σ of the largest amount of $SrCl_2$ we added is less than 0.01.

Table 1. Solution recipes for supersaturated growth fluids.*

σ	Range in [Sr]	$[CaCl_2] \times 10^4$	$[NaHCO_3] \times 10^3$	$\alpha_{Ca}2+ \times 10^5$	$\alpha_{CO3}2- \times 10^5$	No. of separate samples
0.55	0 to 0.45×10^{-4}	2.45	7.45	7.56	7.62	3
0.67	0 to 1.80×10^{-4}	2.60	7.85	7.99	8.02	1
0.76	0 to 2.25×10^{-4}	2.75	8.25	8.41	8.43	4
0.93	0 to 3.00×10^{-4}	3.00	9.00	9.10	9.18	2
1.17	0 to 3.00×10^{-4}	3.42	10.24	10.24	10.28	8

* Recipes calculated with Geochemist's Workbench with solubility constants of Plummer and Busenberg (1982). All concentrations and activities are given in molal, and σ is defined as in Eqn. 1. Every solution contained 0.1 molal NaCl, and pH was adjusted to 8.5 by NaOH addition.

2.2. Direct Nanoscale Measurement of Calcite Growth

Growth dynamics were quantified in situ as calcite precipitated from supersaturated solutions onto seed crystals. Direct observation and measurements were made by AFM, using a Digital Instruments Nanoscope IIIa in contact mode. Growth solutions flowed continuously at 30 mL/h from a syringe pump through an O-ring–sealed fluid cell containing a sample seed crystal. Previous experiments by Teng et al. (1998) with an identical apparatus demonstrated that step speed is independent of fluid flow rate above 25 mL/h; thus we believe that growth is limited not by diffusive transport but by surface processes in these experiments. Samples were freshly cleaved fragments of natural calcite, $\sim 2 \times 2 \times 0.5$ mm in size, upon which overgrowths of calcite were precipitated from supersaturated solutions. These experiments were conducted at ambient temperature, which varied from ~23° to ~25°C, measured in the AFM head. Growth hillock morphology and migration rates of monomolecular steps were imaged and measured in near real time using the methods of Teng et al. (2000).

Experiments were performed for each level of supersaturation by first locating appropriate growth features in Sr-free solution and then successively introducing batches of solution with different Sr concentrations. Normally Sr concentration was monotonically increased while a given growth feature was observed and measured. For all supersaturation levels except $\sigma = 0.93$, however, data were collected a few points at a time from separate samples on more than one day. Thus the data reported below represent results from replicate experiments, and the order in which Sr concentrations were measured was not always the same.

The system was allowed at least 20 min after introduction of each new solution, after which step speeds were observed to be nearly constant over time. Step speeds were calculated in each case from a series of image captures over several minutes to ensure that growth rate was essentially constant. Thus hundreds of steps were generated before data were collected at each condition. We did not observe cessation of growth after the first Sr-bearing step owing to abrupt changes in lattice parameters as seen by Astilleros et al. (2003). In addition, we can be certain that cessation of growth in our high-Sr experiments was not due to nucleation of a Sr-rich orthorhombic carbonate phase on the surface; as we will discuss below, the Sr concentration at which growth stops is positively correlated with supersaturation. If strontianite nucleation were responsible for halting growth, we would expect this correlation to be negative.

2.3. Differential Segregation Experiments

Fragments of natural calcite $\sim 2 \times 2 \times 0.5$ mm in size were cleaved with a razor blade along [104] faces as seeds for crystallization. Samples were placed in Plexiglas fluid cells identical in shape and size to the AFM fluid cell, but without cantilevers. Growth solutions were injected by syringe pump at 30 mL/h from two parallel syringes, one containing dissolved $NaHCO_3$ and the other containing NaCl, $CaCl_2$, and $SrCl_2$. The two solutions mixed as they were injected through a manifold and Teflon tubing on the way to the sample chambers. Solution concentrations were chosen to duplicate the levels of supersaturation used for AFM experiments upon mixing of the two components, and fresh $NaHCO_3$ was loaded twice daily to avoid possible decarbonation, although the system was closed. Before the start of each experiment, aliquots of the $NaHCO_3$ and chloride salt solutions were mixed and adjusted to a pH of 8.50 with several microliters of 1 M NaOH. An appropriate amount of NaOH was then added to the remaining chloride solution so that pH would be fixed near 8.5 throughout the experiment. The pH of the mixed solution was checked twice daily and was always 8.50 ± 0.05. Syringe pumps, tubing, and fluid cells were assembled inside an incubator for precise temperature control at 23.0°C–24.0°C.

Overgrowths of calcite grew on the seed crystals from Sr-bearing solutions for 80 ($\sigma = 0.93$) and 56 hours ($\sigma = 0.67$). The latter sample was initially grown in Sr-free solution with $\sigma = 1.9$ for 18 hours to promote growth and coalescence of growth spirals. A few large features were already present when Sr-bearing solution was introduced. Based on growth rates measured by AFM, these experiments were long enough to produce overgrowths at least 2 microns thick. Once removed from the fluid cells, the samples were attached to glass slides with cyanoacrylate-based adhesive or double-sided carbon tape and then carbon coated for electron microprobe analysis.

Concentrations of strontium in the calcite overgrowths were determined using the Cameca SX-50 electron microprobe in the Department of Geosciences at Virginia Tech. Rectangular grids of spot analyses were collected across single growth hillocks at 5–7 μm intervals. X-rays were counted using an accelerating voltage of 10 kV and a 20 nA beam current for 60 s on the Sr Lα peak and 20 s at each background position. Synthetic $SrCO_3$ was analyzed as a standard. Ca α was counted for 20 s on the peak and 10 s on each background to check analysis totals. A sample grown in Sr-free solution contained amounts of Mg, Mn, and Sr below detection limits. Data reduction for all analyses is based on the methods of Pouchou and Pichoir (1985).

3. RESULTS

3.1. Step Flow Rates as a Function of Fluid Strontium Concentration

We made kinetic measurements of calcite growth from AFM images according to the methods of Teng et al. (2000) for solutions with σ from 0.55 to 1.17 and fluid [Sr] from 0 to 3×10^{-4} molal. Data are listed in Table 2. Throughout the range of conditions investigated, the layer growth mechanism was observed directly as monomolecular step propagation from spiral dislocations or other defects, and calcite was the only mineral phase observed to precipitate.

The inclined orientation of carbonate groups in the calcite lattice with respect to [104] faces leads to two geometrically distinct step types on [104] surfaces. Consequently, calcite growth hillocks comprise four stepped flanks, two with acute angles between step risers and terraces (−) and two with obtuse angles (+):

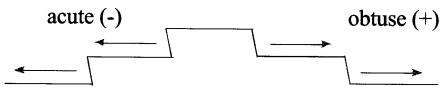

Further description is included in the caption to Figure 3 and in Teng et al. (1999).

Table 2. Measured step speeds for all atomic force microscopy experiments (data from Wilson, 2003).

σ	[Sr] $\times 10^4$ (m)	v_+ (nm/sec)	v_- (nm/sec)
0.55	0.00	4.41	4.09
0.55	0.00	4.59	3.30
0.55	0.30	1.51	1.83
0.55	0.30	4.75	4.18
0.55	0.45	0.06	0.57
0.67	0.00	7.57	3.91
0.67	0.30	7.28	4.87
0.67	0.60	7.93	4.50
0.67	0.90	7.38	5.22
0.67	1.20	8.62	5.11
0.67	1.50	5.60	4.70
0.67	1.80	0.31	2.03
0.76	0.00	8.17	5.49
0.76	0.30	8.13	5.92
0.76	0.60	8.82	6.64
0.76	0.90	8.92	6.16
0.76	1.20	9.51	7.84
0.76	1.50	8.85	7.80
0.76	1.80	7.42	7.90
0.76	1.80	8.43	6.77
0.76	1.95	7.78	7.58
0.76	2.10	6.16	7.24
0.76	2.10	0.78	3.38
0.76	2.25	0.09	0.92
0.93	0.00	10.76	4.75
0.93	0.00	9.89	4.72
0.93	0.90	10.44	6.32
0.93	1.80	10.74	7.65
0.93	2.40	9.31	7.24
0.93	2.70	7.66	7.43
0.93	3.00	0.45	2.80
1.17	0.00	12.38	5.98
1.17	0.00	13.03	6.95
1.17	0.00	13.98	6.98
1.17	0.99	17.21	9.05
1.17	1.50	15.92	11.94
1.17	1.98	15.83	11.10
1.17	2.25	15.73	14.58
1.17	2.55	14.65	10.68
1.17	3.00	15.34	12.89
1.17	3.00	13.07	9.94

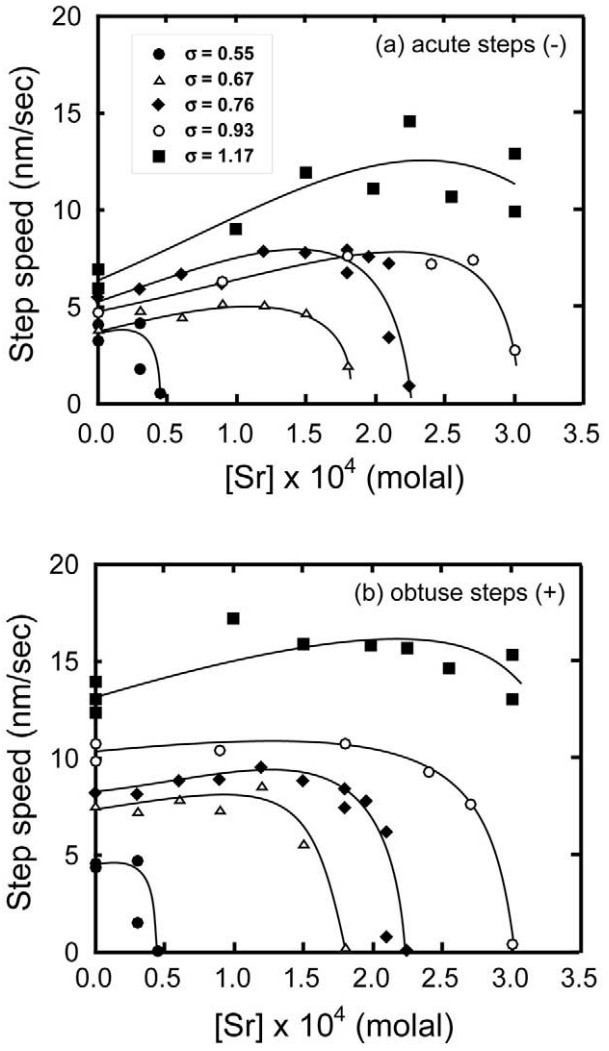

Fig. 1. Step speeds as a function of fluid strontium concentration for five degrees of supersaturation (σ) for (a) acute steps and (b) obtuse steps. Each point represents a step speed measurement made during steady-state growth in the indicated solution; curves are hand drawn to fit the data trends.

Step migration rates are plotted as a function of fluid strontium concentrations for acute and obtuse step directions in Figure 1a and b, respectively. At these values of σ, rates of step migration are higher for obtuse (+) steps than for acute (−) steps, consistent with Teng et al. (1999). Obtuse step speeds in the Sr-free experiments increase from 4.4 nm/s at $\sigma = 0.55$ to nearly 14 nm/s at $\sigma = 1.17$, and acute step speeds range from 3.3 to ~7 nm/s over the same interval.

Rigorous estimation of uncertainties for these experiments is extremely difficult. Standard errors for the measurement of step speeds from AFM images can be calculated and are on the order of a few tenths of nm/s. Other sources of variation, however, such as variations in solution composition, degassing, or CO_2 or the presence of minute quantities of unknown impurities are impossible to measure in situ and likely make larger contributions to overall uncertainties. For this reason, error bars are not shown in the graphs, but uncertainties are conservatively estimated as ±3 nm/s for all experiments, though they are likely smaller. Step speeds have been systematically corrected for friction between scanner, O-ring, and fluid cell for growth hillocks near the center of the AFM scanner's range of motion, but increased friction when imaging features near the limits of that range may lead to overestimates of step speed by a few percent relative.

With incremental addition of low levels of Sr to growth solutions, we found that step speeds increase. For example, at $\sigma = 0.76$, step speed for acute steps increased from an average of 5.3 nm/s in the Sr-free system to 7.9 nm/s at a total Sr concentration of 1.8×10^{-4} molal. Likewise, step speed increases from an average of 6.6 nm/s in the pure system to maximum of 14.6 nm/s with 2.25×10^{-4} molal Sr at $\sigma = 1.17$. Similar trends are observed for other values of σ and for obtuse step migration rates. The concentration of Sr resulting in maximum step speed for each trend is positively correlated overall with degree of supersaturation.

To make this trend clear despite scatter in the data and subtlety of the increase in step speed with Sr addition, we show

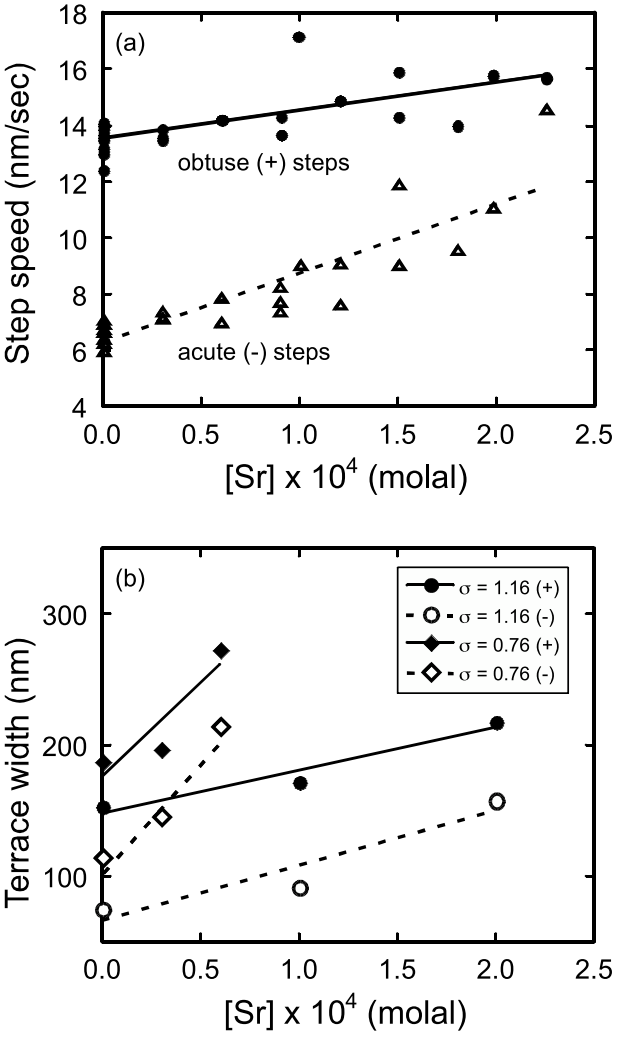

Fig. 2. (a) Ignoring the points where step speed is obviously retarded by high Sr concentrations, acute step speed data from Figure 1a were shifted up such that the five trends share a common Sr-free intercept (filled circles). A linear fit to these grouped points has $R = 0.68$. Data from Figure 1b are also shown in the same panel as open triangles, with $R = 0.88$. (b) Terrace widths vs. fluid Sr concentration for selected experiments.

all the data together in Figure 2a. To construct this plot, we fit a line to the acute (−) step data for each saturation level, ignoring the points where growth is drastically retarded by high levels of Sr (see below). This resulted in five linear fits with various intercepts at [Sr] = 0, one for each saturation level. We then shifted all the raw data points up (added to step speed), so that all five lines in each set had the same intercept. We then plotted all the data together and fitted a single line representing the overall increase in step speed as a function of [Sr], averaged for all saturation levels. Data for obtuse (+) steps have been similarly normalized and plotted together in the same plot. At low Sr concentrations, terrace widths consistently increased with Sr addition for both obtuse and acute step types. A subset of the terrace width data is shown in Figure 2b.

Higher levels of Sr have a strong inhibitory effect on step speeds. For each value of σ, there is a particular concentration of Sr above which calcite steps decrease in speed extremely rapidly and, upon additional Sr input, cease to propagate. The concentrations of Sr that result in zero or near-zero step speeds are positively correlated with σ, ranging from 4.50×10^{-5} molal at $\sigma = 0.55$ to 3.00×10^{-4} molal at $\sigma = 0.93$ to $>3.00 \times 10^{-4}$ molal at $\sigma = 1.17$.

3.2. Step Migration Rates as a Function of Supersaturation

Step speeds are plotted as a function of σ in Figure 3. This figure was generated from the data in Figure 1 by selecting several Sr concentrations and taking the step speeds at each σ from the hand-drawn curves. The Sr-free points define a linear trend, with step speed increasing from ~3 nm/s at $\sigma = 0.55$ to ~7 nm/s at $\sigma = 1.17$ molal for acute (−) steps and from ~4 to ~13 nm/s over the same range in σ for obtuse (+) steps. Each

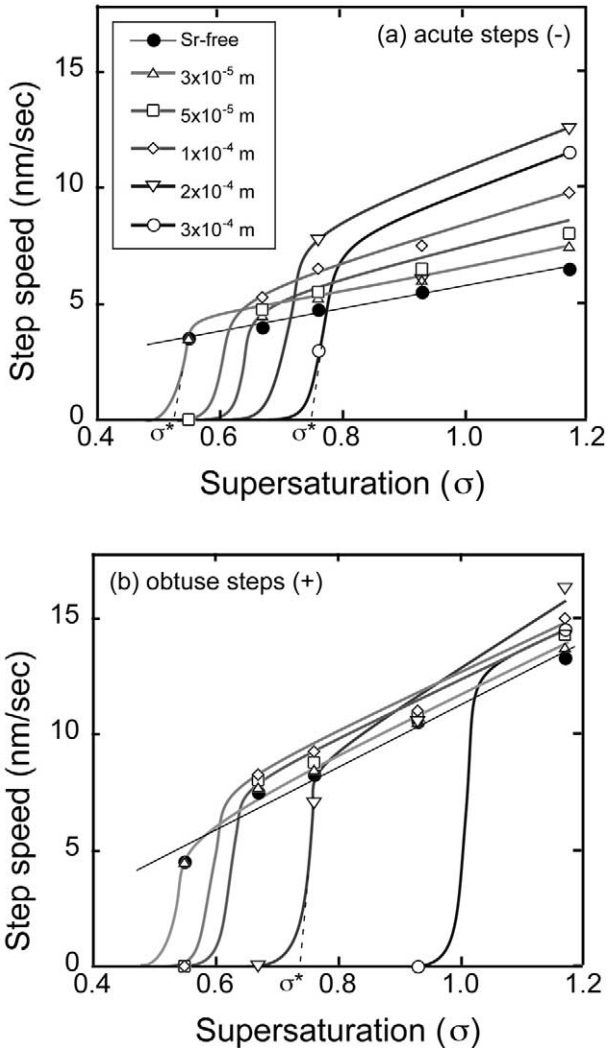

Fig. 3. Step speeds as a function of supersaturation at nearly constant strontium concentrations for (a) obtuse step directions and (b) acute step directions. This figure was generated by reading step speeds from Figure 1 at selected values of fluid [Sr]. Curves were drawn by hand. On one trend in each plot, σ^*, the critical level of supersaturation needed to initiate growth in the presence of Sr, is explicitly indicated. For clarity, σ^* is not shown for other trends.

Sr-bearing trend has two changes in slope, one defining a threshold value of σ (referred to as σ^* and discussed later), below which no growth occurs. The other is above the trend for the Sr-free system, within the range of conditions where growth in the presence of Sr is faster than in the pure system. Viewing the data in this way makes it possible to see the degree of supersaturation necessary to initiate growth at a given [Sr] (σ^*). In the Sr-bearing system, a value of σ higher than σ^* for a given [Sr] results in faster step migration than observed in the corresponding Sr-free solution.

3.3. Hillock Morphology

Calcite growth in the pure system generated growth spirals with straight step edges parallel to the Miller-indexed vectors [4$\bar{8}$1] and [44$\bar{1}$], as in Paquette and Reeder (1995) and Teng et al. (1998). Incremental addition of Sr leads to significant changes in hillock morphology, as shown in Figure 4. At low Sr concentrations, shown in Figure 4a, terrace widths are slightly wider than in the impurity-free controls (also see Fig. 2b), but the step edges and hillock flanks remain straight and distinct and oriented as in the Sr-free system. At higher Sr concentrations, hillocks become elongate perpendicular to the projection of the calcite *c*-glide plane (Fig. 4b). Acute (−) steps become scalloped. Obtuse (+) steps become scalloped and roughened on a fine scale, and the boundary between the two obtuse-stepped flanks begins to disappear. The two obtuse step directions are gradually replaced by a new step direction with edges parallel to the vector [010].

3.4. Segregation Experiments

Figure 5 shows results from two segregation experiments. Note that the levels of Sr measured reflect a combination of equilibrium and kinetic controls on Sr incorporation. Each of the two images in Figure 5 is a color contour map of Sr concentration in a single growth hillock. The degree of supersaturation was $\sigma = 0.67$ for the sample in Figure 5a and $\sigma = 0.93$ in Figure 5b, but both solutions had a fluid Sr concentration of 5×10^{-5} molal. Results are summarized in Table 3. Sr content of calcite by weight in the experiment with $\sigma = 0.67$ and [Sr] $= 5 \times 10^{-5}$ molal is ~3200 ppm in the obtuse-stepped (+) flanks and ~2000 ppm in the acute-stepped flanks. The experiment with $\sigma = 0.93$ and [Sr] $= 5 \times 10^{-5}$ molal has ~8500 ppm in the obtuse flanks and ~5500 ppm in the acute flanks. These results show that although the fractionation ratio of Sr between obtuse and acute flanks is the same to within experimental error for these two experiments, the absolute Sr levels are significantly larger for the higher growth rate.

4. DISCUSSION

4.1. Enhanced Growth at Low Levels of Added Strontium

We now return to the ability of low levels of Sr to increase rates of step migration on growing calcite surfaces. We examine two possible explanations for enhanced growth in the presence of Sr and compare these in Figure 6, given that step flow rate is described by the equation

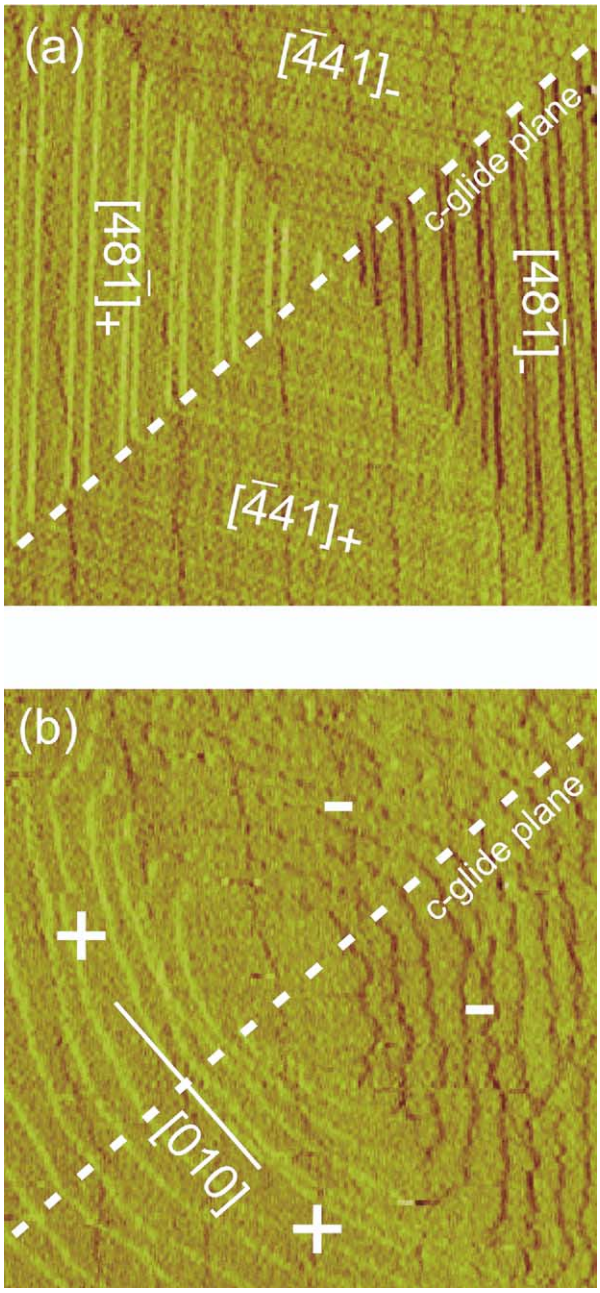

Fig. 4. Terrace widths vs. fluid Sr concentration for two levels of supersaturation. (a) Spiral growing in a solution with $\sigma = 0.93$ and [Sr] $= 1.5 \times 10^{-5}$ molal. The four flanks of the calcite growth hillock are labeled with Miller indices of vectors parallel to the step edges. Note that two of the flanks, labeled +, have obtuse angles on the step risers and are geometrically equivalent across the projection of the calcite *c*-glide plane. The other two flanks (−) have acute angles at the step risers and are geometrically distinct from the obtuse-stepped flanks. (b) Same growth hillock after introduction of solution with $\sigma = 0.93$ and [Sr] $= 4 \times 10^{-5}$ molal. Extreme rounding of the (+) flanks and (+/+) edge have resulted in a new step direction with step edges parallel to [010]. Both AFM images are 2.5 microns across.

$$v = \beta\omega(a_{Ca^{2+}} - a_{Ca^{2+}eq}) \quad (2)$$

(Burton et al., 1951; Chernov, 1961), where v is the step speed (either obtuse or acute), and ω is the molecular volume of the

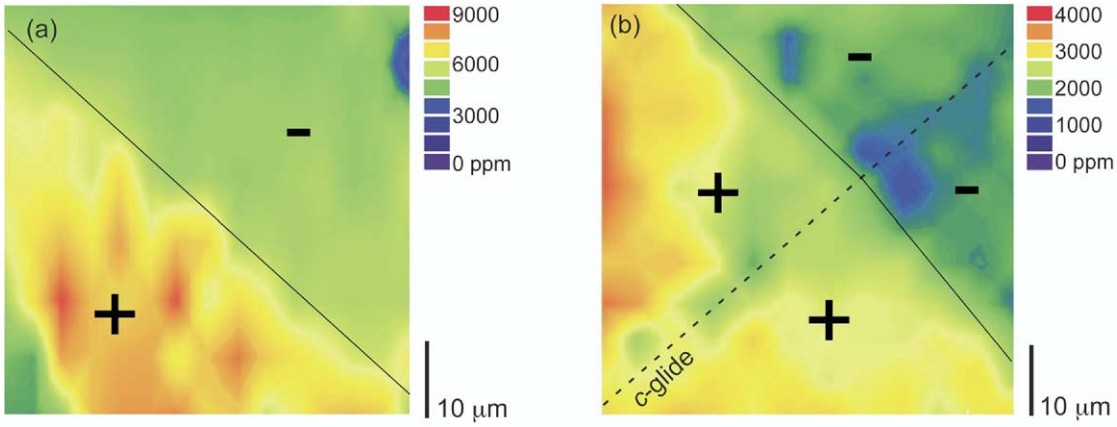

Fig. 5. Concentration map for Sr in calcite from two segregation experiments. (a) $\sigma = 0.67$, fluid [Sr] $= 5 \times 10^{-5}$ molal. (b) $\sigma = 0.93$, fluid [Sr] $= 5 \times 10^{-5}$ molal. Maps were constructed from grids of single-point electron microprobe analyses spaced a few microns apart across each growth hillock. Note that scales differ by slightly more than a factor of two. Obtuse- (+) and acute-stepped (−) flanks are marked, as is the projection of the *c*-glide plane in (b). The grid in (a) was situated somewhat distally on two flanks of a very large growth hillock with multiple defects at the apex; the *c*-glide plane is out of the image area to the upper left.

solid (6.13×10^{-23} cm^3 for pure calcite). One possibility is an increase in the thermodynamic driving force for precipitation, perhaps through a simple increase in effective supersaturation, $a_{Ca^{2+}} - a_{Ca^{2+}eq}$. If the solubility of calcite in solid solution with a small amount of $SrCO_3$ were less than that of pure calcite, then the solubility product, K_{sp}, would be lower, and likewise the equilibrium activity of Ca^{2+} ($a_{Ca^{2+}eq}$) would be smaller. Thus effective supersaturation, ($a_{Ca^{2+}} - a_{Ca^{2+}eq}$), would be larger.

In theory it is possible to determine changes in $a_{Ca^{2+}eq}$ as a function of fluid Sr concentration from our experimental data. Decreases in $a_{Ca^{2+}eq}$ as some Sr^{2+} is incorporated into the calcite structure would ideally produce a set of trends in step speed vs. $a_{Ca^{2+}}$ parallel to the pure system trend similar to the trend in step speed vs. σ shown in Figure 3 but offset toward lower values of $a_{Ca^{2+}}$. The $a_{Ca^{2+}}$-intercepts of these lines yield the values of $a_{Ca^{2+}eq}$ as a function of fluid [Sr]. We have estimated the magnitude of change in $a_{Ca^{2+}eq}$ that would be required to account for the observed increase in step speeds with addition of low levels of Sr in the following way.

For each value of σ studied experimentally, we determined the slope and intercept of the best fit line to trends in obtuse step speed vs. fluid [Sr], while carefully excluding those points outside the region of enhanced growth at low [Sr]. We then used the five resulting intercepts to shift all points such that those five lines share a common intercept. A single line was then fit to all data and its slope taken to be the dependence of step speed on fluid [Sr] for the whole data set. The five original intercepts, representing pure system step speeds, and the single slope can be used to generate linear curves for step speed vs. $a_{Ca^{2+}}$ for several arbitrarily chosen concentrations of Sr, as shown in Figure 6a. The intercepts of these lines along the activity axis yield $a_{Ca^{2+}eq}$ as a function of fluid [Sr] as follows:

$$a_{Ca^{2+},eq} = 5.9 \times 10^{-5}\,\mathrm{m} - 3.3 \times 10^{-2}\,[\mathrm{Sr}]. \quad (3)$$

Thus, over the full range of [Sr] studied, equilibrium activity would need to vary only ~3% to account for the observed increases in step speed with Sr addition. The result for acute steps is very similar. Because the required shift in $a_{Ca^{2+}eq}$ is so slight, extremely precise experimental data are necessary to determine with certainty whether such a shift in solubility is indeed responsible for the observed growth enhancement. Despite the difficulty of making this estimate with the present data, we can say that the shift in solubility needed to account for the observed increases in growth rate is on the order of a few percent.

If incorporation of Sr causes an increase in effective supersaturation (σ_{eff}) by lowering $a_{Ca^{2+}eq}$, then our results imply a concomitant thermodynamic change upon Sr addition. The width of terraces on growth hillocks is proportional to the ratio $G\gamma/\sigma_{eff}$, where G is the Gibbs factor, related to curvature-induced retardation of steps with very short edge length, such as near the apex of a growth spiral, and γ is the step-edge free

Table 3. Results from Sr segregation experiments.

σ	Fluid [Sr] (molar)	Fluid Sr/Ca (molar)	Flank	Sr conc.* (ppm)	mol Sr/mol calcite	Segregation coefficient‡
0.67	5×10^{-5}	0.192	obtuse (+)	3200	0.0037	0.019
			acute (−)	2000	0.0023	0.012
0.93	5×10^{-5}	0.167	obtuse (+)	8500	0.0097	0.058
			acute (−)	5500	0.0063	0.038

* Uncertainties are <200 ppm.
‡ $(Sr_{calcite}/Sr_{fluid})/(Ca_{calcite}/Ca_{fluid})$.

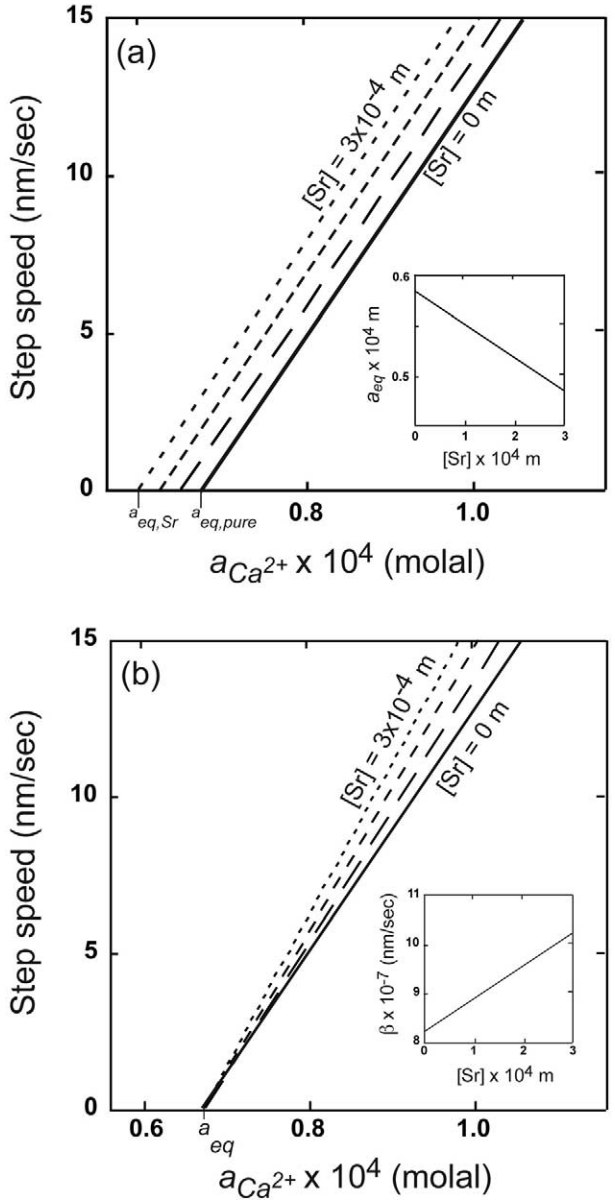

Fig. 6. Comparison of thermodynamic and kinetic effects that would be required to cause the observed growth enhancement. (a) Calculated trends in step speed vs. $a_{Ca^{2+}}$ based on experiments where growth is enhanced by the presence of Sr. If growth enhancement by Sr is due to lowering the solubility of calcite by incorporation of small amounts of Sr, then the intercepts of these linear fits along the activity axis yield the equilibrium activity for Sr-bearing calcite as a function of fluid Sr concentration. The required change in equilibrium activity is only ~3% relative for the range of Sr concentrations studied (see text for details). (b) Calculated trends in kinetic coefficient, β, as a function of $a_{Ca^{2+}}$. This is also based on linear fits to the experimental data that display enhanced growth relative to the Sr-free system, but here the acceleration is assumed to be a kinetic effect. A change in β of ~10% relative would account for the observed growth enhancement (see text).

energy (see Teng et al., 1998, and references therein). If Sr addition simply causes an increase in σ_{eff}, then terrace widths should decrease as Sr concentration increases, but in our experiments terrace widths *increase* with increasing Sr (Fig. 2b). Therefore any increase in σ_{eff} must be accompanied by a proportionally larger increase in the product Gγ. Which of G and γ might be increasing and how Sr affects these thermodynamic parameters remain unknown.

An alternative to decreased solubility is that the increase in step speeds is a kinetic effect of Sr addition. To assess this possibility, we look for increases in the kinetic coefficient, β, in Eqn. 2. Increasing values of β with Sr addition would imply that impurity cations cause faster attachment or reduced detachment of new growth units, the vast majority of which contain Ca, not Sr. We do not yet have a mechanistic explanation for how this might be accomplished, but one possibility is that Sr increases the density of kink sites along step edges (step roughening), thus increasing the density of sites where new growth units can attach. Relative to other systems, calcite step edges tend to be smooth, such that growth rates are limited by kink availability under some conditions (Teng et al., 1998; De Yoreo and Vekilov, 2003).

We have estimated the change in β required to account for the observed step speeds (see Fig. 6b) by applying the same fits to step speed vs. fluid [Sr] used to generate Figure 6a. This time the value of $a_{Ca^{2+}} - a_{Ca^{2+}eq}$ was held constant and β was allowed to vary as a function of [Sr] to fit the observed increase in step speeds. From the slopes of the lines shown in Figure 6b we can express β as a function of fluid Sr concentration. For Sr concentrations low enough relative to calcite supersaturation to cause growth faster than that observed in the Sr-free system,

$$\beta = 3.04 \times 10^5 \mathrm{nm/sec} + 2.5 \times 10^8 \mathrm{nm \cdot kg/mol \cdot sec[Sr]} \quad (4)$$

A relative change in β of ~10% over the range of conditions studied would account for that phenomenon. In summary, because the changes in $a_{Ca^{2+}} - a_{Ca^{2+}eq}$ or β needed to cause faster growth in the presence of Sr are very slight, the imprecision of experimental data does not enable us to conclude whether this is attributable to thermodynamic, kinetic, or combined effects. Precise determination of the solubility of solid-solution calcite crystals as a function of Sr content might help to discriminate between the possible causes of growth enhancement.

4.2. Growth Inhibition at Higher Sr Concentrations

As fluid [Sr] increases beyond the regime where growth is enhanced, growth is strongly inhibited and very quickly stopped altogether, as evident in Figure 1. This sudden growth inhibition suggests pinning or blocking of steps by adsorption of impurity ions as typically described by the classic model of Cabrera and Vermilyea (1958). Within this model, when the average spacing of adsorbed impurities along a step edge is less than two times this critical length, i.e., the minimum step length required for step motion, the step is unable to propagate beyond the "fence" of adsorbed impurities (Potapenko, 1993; De Yoreo and Vekilov, 2003). Because the critical length is inversely proportional to supersaturation (Burton et al., 1951), the threshold concentration of impurity ions needed to block advancement of steps increases with supersaturation. From Figures 1 and 3, one might expect the Cabrera and Vermilyea model to explain the data. However, although the analysis is beyond the scope of this paper and will be presented elsewhere, we find that the model dramatically fails to describe the abrupt decrease

in growth rate at a critical saturation-dependent Sr level. Similar behavior is observed for calcite growth in the presence of acidic dipeptide molecules (Han et al., 2004) and KH_2PO_4 in the presence of Al^{3+}, Fe^{3+}, or Cr^{3+} (Thomas et al., 2004). While it is unlikely that Sr concentrations in biomineralizing fluids are ever high enough to halt growth in this way, this kind of step-blocking mechanism, perhaps in the presence of peptides, may indeed be an important way that organisms regulate mineral growth and morphology.

4.3. Sr Content Varies with Fluid Supersaturation

Our electron microprobe measurements of Sr in calcite grown by monolayer step propagation clearly demonstrate that the extent of impurity incorporation is strongly influenced by step-specific geometry, as is evident in the contour plots of Figure 5. This result and the strong preference of Sr for obtuse subsectors of growth hillocks agree qualitatively with previous work by Paquette and Reeder (1995) but constrast with the prediction made by the molecular dynamics model of de Leeuw et al. (2002). We also find that our sample with $\sigma = 0.93$ has approximately twice as much Sr in the calcite as that with $\sigma = 0.67$. Fluid [Sr] was the same for both experiments, but the higher supersaturation solution contained 15% more Ca. Nonetheless, the high supersaturation sample contains more Sr despite a lower Sr/Ca ratio in solution. This effect may be a result of excess impurity entrapment because steps are moving more quickly and incorporating a larger proportion of adsorbed impurities (Chernov, 1962; Watson, 1996, 2004), but it could also be due to higher carbonate content, which has been anecdotally observed to correlate with impurity content (Boyle and Erez, 2004).

Because Sr is strongly fractionated between obtuse and acute steps, we have estimated two segregation coefficients for each of the two experimental conditions presented above. For $\sigma = 0.93$, these coefficients, defined as $(Sr_{calcite}/Sr_{fluid})/(Ca_{calcite}/Ca_{fluid})$, molar, are 0.058 and 0.038 for obtuse and acute subsectors, respectively. For $\sigma = 0.67$, they are 0.019 and 0.012, respectively. Direct comparison with some previous studies, e.g., Mucci and Morse (1983) and Paquette and Reeder (1995), is not possible because those experiments involved multiple impurities or because supersaturation and fluid [Sr] were unknown. However, Sr contents of our experiments are quite a bit higher than those of Paquette and Reeder (1995), although fractionation between obtuse and acute vicinal faces is comparable. Tesoriero and Pankow (1996) conducted bulk powder experiments with much higher supersaturation than we had. In bulk experiments, growth mechanism is unknown, and the dependence of Sr segregation on growth rate very near equilibrium is difficult to resolve. Nevertheless, they report a strong dependence on growth rate and a bulk segregation coefficient for Sr of 0.021 at the lowest growth rates. Our results are in good agreement with theirs. Their dramatically higher values obtained at the fastest growth rates may be caused in part by a change in growth mechanism at high supersaturation from layer growth to 2D nucleation or a mixture of the two. Lorens (1981) also found a positive correlation between Sr incorporation and growth rate and slightly higher values for D_{Sr} than either ours or that of Tesoriero and Pankow.

4.4. Hillock Morphology

Scalloping of the obtuse and acute step edges at high Sr concentrations is likely the morphologic manifestation of step pinning by impurity ions (De Yoreo and Vekilov, 2003). Finer scalloping along obtuse step edges may be indicative of more-closely spaced Sr cations along those step edges than along acute step edges, which is consistent with our observation of higher Sr contents in obtuse flanks of the calcite crystals. Also, the observed changes in hillock shape, particularly the pronounced rounding of obtuse step edges and disappearance of the (+/+) boundary, may be related to a zone of low Sr observed along the projection of the *c*-glide plane (Fig. 5b; other hillocks not shown; this feature is not visible in Fig. 5a because that particular region contains only two flanks of one very large hillock). Speculation about the nature of this connection is difficult, but, thinking in terms of characteristic lifetimes of impurities at step edges, one possibility is that the energy penalty for incorporating Sr cations at the (+/+) or (−/−) boundary is particularly large. Sr cations that adsorb at that boundary have a lower probability of being incorporated as the steps advance but the same average residence time as adsorbed impurities elsewhere. The (+/+) boundary can only advance once the adsorbed impurities desorb or are incorporated; thus the step speed is slower here. Slow migration of the (+/+) corner eventually leads to formation of steps with edges parallel to [010], which is a previously identified periodic bond chain in the calcite structure (Heijnen, 1985; Reeder and Rakovan, 1999). Note that these morphologic changes are neither observed nor expected in the samples analyzed for Sr incorporation above. Sr levels in those experiments were relatively low, because they are in the regime where growth is accelerated by presence of Sr and where morphologic effects are not observed by AFM, whereas the hillock shown in Figure 4b is in relatively Sr-rich solution.

Davis et al. (2004) discuss a possible connection between microscopic hillock morphology changes induced by Mg and a trend towards macroscale elongation along the *c*-axis to form prismatic crystals, as observed by Folk (1974). This prediction is independently confirmed by Han and Aizenberg (2003). Changes in crystal habit due to Sr are not known, because calcite crystals with significant amounts of Sr are rare, and Sr-rich calcite normally contains even larger amounts of Mg. However, if the new [010] step direction we see in our hillocks in the presence of Sr were extrapolated to the macroscopic scale, we would expect shortening along the *c*-axis and formation of a [001] face.

5. CONCLUDING REMARKS

Our in situ AFM measurements of calcite growth show that Sr causes complex changes in the rate of monolayer step flow and, at higher concentrations, alters step edge orientations to yield growth hillocks with a unique morphology. In parallel experiments, electron microprobe analyses show that Sr contents at the hillock scale are highly specific to the two types of crystallographically controlled step directions. Sr in calcite is fractionated between obtuse- and acute-stepped flanks by a factor of approximately two, and Sr incorporation is strongly correlated with solution supersaturation.

The experimental design in our investigation enabled us to couple the in situ AFM measurements and microprobe data to yield several new insights into factors that control Sr signatures in calcite. First, the rate data show that, at low concentrations, Sr promotes faster growth. The phenomenon of steady-state, accelerated growth due to impurities is previously undocumented. This effect may be associated with slight shifts in calcite solubility when Sr is incorporated or may be due to as yet uncharacterized kinetic effects. In either case, our nanoscale observations show that growth morphology is unaffected at low Sr levels and supersaturations. Our experiments do not consider Sr effects on calcite growth in the presence of the many impurities contained in seawater, but, taken alone, our findings indicate that the small concentrations of Sr that occur in marine waters can be expected to enhance growth rate but are unlikely to cause significant modification to the macroscopic growth morphology. As discussed in the paper, we cannot yet assess whether the Sr-induced rate increase is rooted in a kinetic or thermodynamic effect (or both). This problem is presently being addressed in ongoing work.

Second, while geochemists have long correlated impurity levels with growth rate, to our knowledge none have demonstrated this dogma with certainty. To do so requires that a single growth mechanism prevail across the observed range of supersaturations. Teng et al. (2000) show that, for calcite, a transition from the layer growth mechanism to surface nucleation mechanisms occurs at σ as low as 1.5, yet many previous studies using batch reactors employed supersaturations as high as 5 to 30 (e.g., Katz, 1972; Lorens, 1981; Mucci and Morse, 1983; Tesoriero and Pankow, 1996). At these conditions, the effects of two-dimensional nucleation or mixed growth mechanisms would have been folded into conclusions regarding "apparent" impurity contents. By knowing the growth mechanism through direct observation and determining Sr contents from individual growth hillocks, we found that Sr levels are strongly correlated with step flow rate for this single near-equilibrium growth mechanism. This may give insight to interpreting Sr signatures measured in field calcites, because it implies that under some conditions, supersaturation (one proxy for growth rate) has a primary control on Sr contents. The sensitivity of Sr uptake to supersaturation may explain apparently contradictory results in the literature regarding whether Sr incorporation in the calcite produced by one-celled marine organisms is controlled by temperature (see Section 1). Our findings suggest that Sr contents of natural calcite samples may be a good indicator of the relative supersaturations at which the crystals grew without necessarily revealing other information. More work is needed to further this understanding.

Third, at the higher Sr levels used in our study, step advancement stops by pinning kink-sites or step edges. The threshold Sr concentration needed to halt growth is positively correlated with supersaturation. Further analysis of the data is needed to develop a theoretical model that gives a robust quantitative description of Sr behavior and the similarly abrupt growth-halting effect recently observed for polyaspartate- and dipeptide-calcite interactions (Han et al., 2004). The failure of classic crystal growth models to describe this behavior suggests that an underlying principle exists that we do not yet understand.

Finally, results of this investigation demonstrate that understanding the impurity-specific interactions with calcite growth surfaces at the microscopic scale is of high importance. A good example of this is found in Mg and Sr, which have many similar geochemical characteristics yet clearly have very different modes of calcite growth modification. In contrast to the Sr behavior reported in this paper, Mg inhibits growth through incorporation to produce a Mg-calcite solid solution mineral with a higher apparent solubility (Davis et al., 2000; Davis et al., 2004) and causes a very different morphologic effect on growth structures (Davis et al., 2004). Clearly, the science that underlies growth modification by impurities is an area that warrants more thorough understanding. If Sr and other impurities are to be used as robust indicators of growth conditions for natural calcite samples, well grounded knowledge of the mechanisms for recording trace element signatures in calcite is an essential step toward accurately inferring paleoenvironmental signals from fossil calcite compositions.

Acknowledgments—This study was supported by the NSF Division of Chemical Oceanography (OCE-0083173) and the DOE Office of Basic Energy Sciences, Division of Chemical Sciences, Geosciences, and Biosciences (FG02-00ER15112). We thank Meg Grantham and Nizhou Han for support with the wet chemistry experiments and Bob Tracy for expert assistance in the microprobe facility at Virginia Tech. We appreciate helpful suggestions from three anonymous reviewers and editorial handling by C. Eggleston.

Associate editor: Carrick M. Eggleston

REFERENCES

Astilleros J. M., Pina C. M., Fernandez-Diaz L., and Putnis A. (2003) Metastable phenomena on calcite [1014] surfaces growing from Sr^{2+}-Ca^{2+}-CO_3^{2-} aqueous solutions. *Chem. Geol.* **193,** 93–107.

Boyle E. A., and Erez J. (2004) Does carbonate ion influence foraminiferal Mg/Ca? *EOS Trans. AGU* **84** (*52*), OS21G–01.

Burton W. K., Cabrera N., and Frank F. C. (1951) The growth of crystals and the equilibrium structure of their surfaces. *Phil. Trans. R. Soc. London Ser. A Math. Phys. Sci.* **245,** 299–358.

Cabrera N. and Vermilyea D. A. (1958) The growth of crystals from solution. In *Growth and Perfection of Crystals* (eds. R. H. Doremus, B. W. Roberts and D. Turnbull), pp. 393–410. Wiley, New York.

Carpenter S. J., and Lohmann K. C. (1992) Sr/Mg ratios of modern marine calcite: Empirical indicators of ocean chemistry and precipitation rate. *Geochim. Cosmochim. Acta* **56,** 1837–1849.

Chernov A. A. (1961) The spiral growth of crystals. *Soviet Phys.* **4,** 116–148.

Chernov A. A. (1962) Excess impurity trapping during crystal growth. In *Growth of Crystals*, Vol. 3 (eds. A. V. Shubnikov and N. N. Sheftal), pp. 35–39. Consultants Bureau, New York.

Cronblad H. G. and Malmgren B. A. (1981) Climatically controlled variation of Sr and Mg in Quaternary planktonic foraminifera. *Nature* **291,** 61–64.

Davis K. J., Dove P. M., and De Yoreo J. J. (2000) The role of Mg^{2+} as an impurity in calcite growth. *Science* **290,** 1134–1137.

Davis K. J., Dove P. M., Wasylenki L. E., and De Yoreo J. J. (2004) Morphological consequences of differential Mg^{2+} incorporation at structurally distinct steps on calcite. *Am. Mineral.* **89,** 714–720.

De Leeuw N. H., Harding J. H., and Parker S. C. (2002) Molecular dynamics simulations of the incorporation of Mg^{2+}, Cd^{2+} and Sr^{2+} at calcite growth steps: Introduction of a $SrCO_3$ potential model. *Mol. Simul.* **28**: 573–589.

De Yoreo J. J., Burnham A., and Whitman P. K. (2002) Developing KDP and DKDP crystals for the world's most powerful laser. *Int. Mater. Rev.* **13,** 233.

De Yoreo J. J. and Vekilov P. G. (2003) Principles of crystal nucleation and growth. In *Biomineralization*, Vol. 54 (eds. P. M. Dove, J. J.

and De Yoreo S.). Weiner Mineralogical Society of America, Washington, D.C.

Delaney M. L., Bé A. W. H., and Boyle E. A. (1985) Li, Sr, Mg, and Na in foraminiferal calcite shells from laboratory culture, sediment traps and sediment cores. *Geochim. Cosmochim. Acta* **49,** 1327–1341.

Elderfield H., Bertram C. J., and Erez J. (1996) A biomineralization model for the incorporation of trace elements into foraminiferal calcium carbonate. *Earth Plan. Sci. Lett.* **142,** 409–423.

Folk R. L. (1974) The natural history of crystalline calcium carbonate: Effect of magnesium content and salinity. *J. Sed. Pet.* **44,** 40–53.

Graham D. W., Bender M. L., Williams D. F., and Keigwin L. D. (1982) Strontium-calcium ratios in Cenozoic planktonic foraminifera. *Geochim. Cosmochim. Acta* **46,** 1281–1292.

Gruzensky P. M. (1967) Growth of calcite crystals. In *Crystal Growth* (ed. H. S. Peiser), pp. 365–367. Pergamon, Oxford.

Han N., Grantham M. C., De Yoreo J. J., and Dove P. M. (2004) An investigation of dipeptide modulation of calcite growth. *Mater. Res. Soc. Spring Meeting Symp. Z.* San Francisco, California.

Han Y.-J. and Aizenberg J. (2003) Effect of magnesium ions on oriented growth of calcite on carboxylic acid functionalized self-assembled monolayer. *J. Am. Chem. Soc.* **125,** 4032–4033.

Heijnen W. M. (1985) The morphology of gel grown calcite. *Neues Jahrbuch für Mineralogie* **1985,** 357–371.

Holland H. D., Holland H. J., and Munoz J. L. (1964) The coprecipitations of cations with $CaCO_3$-II. The coprecipitation of Sr^{2+} with calcite between 90° and 100°C. *Geochim. Cosmochim. Acta* **28,** 1287–1301.

Kahr B. and Gurney R. W. (2001) Dyeing crystals. *Chem. Rev.* **101,** 893–951.

Katz A., Sass E., Starinsky A., and Holland H. D. (1972) Strontium behavior in the aragonite-calcite transformation: An experimental study at 40–98°C. *Geochim. Cosmochim. Acta* **36,** 481–496.

Lea D. W., Mashiotta T. A., and Spero H. J. (1999) Controls on magnesium and strontium uptake in planktonic foraminifera determined by live culturing. *Geochim. Cosmochim. Acta* **63,** 2369–2379.

Lorens R. N. (1981) Sr, Cd, Mn and Co distribution coefficients in calcite as a function of calcite precipitation rate. *Geochim. Cosmochim. Acta* **45,** 553–561.

Martin P., Lea D. W., Mashiotta T. A., Papenfuss T., Sarnthein M., and Spero H. J. (1997) Glacial-interglacial variation in mean ocean Sr? *EOS Trans. AGU* **78** (*46*), F388.

Mucci A. and Morse J. W. (1983) The incorporation of Mg^{2+} and Sr^{2+} into calcite overgrowths: Influences of growth rate and solution composition. *Geochim. Cosmochim. Acta* **47,** 217–233.

Paquette J. and Reeder R. J. (1995) Relationship between surface structure, growth mechanism and trace element incorporation in calcite. *Geochim. Cosmochim. Acta* **59** (*4*),735–749.

Pingitore N. E., Jr., Lytle F. W., Davies B. M., Eastman M. P., Eller P. G., andLarson E. M. (1992) Mode of incorporation of Sr^{2+} in calcite: Determination by x-ray absorption spectroscopy. *Geochim. Cosmochim. Acta* **56,** 1531–1538.

Plummer L. N. and Busenberg E. (1982) The solubilities of calcite, aragonite and vaterite in CO_2-H_2O solutions between 0 and 90°C and an evaluation of the aqueous model for the system $CaCO_3$-CO_2-H_2O. *Geochim. Cosmochim. Acta* **46,** 1011–1040.

Potapenko S. Y. (1993) Moving of step through impurity fence. *J. Cryst. Growth* **133,** 147–154.

Pouchou J. L. and Pichoir F. (1985) "PAP" $\Phi(\rho Z)$ procedure for improved quantitative microanalysis. In *Microbeam Analysis* (ed. J. T. Armstrong). San Francisco Press, San Francisco.

Purton L. M. A., Shields G. A., Brasier M. D., and Grime G. W. (1999) Metabolism control of Sr/Ca ratios in fossil aragonitic mollusks. *Geology* **27** (*12*),1083–1086.

Reeder R. J. and Rakovan J. (1999) Surface structural controls on trace element incorporation during crystal growth. In *Growth, Dissolution and Pattern Formation in Geosystems* (eds. B. Jamtveit and P. Meakin). Kluwer Academic Publishers, Dordrecht, The Netherlands.

Rickaby R. E. M., Schrag D. P., Zondervan I., and Riebesell U. (2002) Growth rate dependence of Sr incorporation during calcification of Emiliania huxleyi. *Global Biogeochem. Cycles* **16,** 61–68.

Rosenthal Y., Boyle E. A., and Slowey N. (1997) Temperature control on the incorporation of magnesium, strontium, fluorine and cadmium into benthic foraminiferal shells from Little Bahama Bank: Prospects for thermocline paleoceanography. *Geochim. Cosmochim. Acta* **61,** 3633–3643.

Smolsky I. L., Voloshin A. E., Zaitseva N. P., Rudneva E. B., and Klapper H. (1999) X-ray topographical study of striation formation in layer growth of crystals from solutions. *Phil. Trans. R. Soc. London Ser. A Math. Phys. Sci.* **357,** 2631–2649.

Stoll H. M., Rosenthal Y., and Falkowski P. (2002) Climate proxies from Sr/Ca of coccolith calcite: calibrations from continuous culture of *Emiliania huxleyi*. *Geochim. Cosmochim. Acta* **66,** 927–936.

Teng H. H., Dove P. M., and DeYoreo J. J. (1999) Reversed calcite morphologies induced by microscopic growth kinetics: insight into biomineralization. *Geochim. Cosmochim. Acta* **63** (*17*),2507–2512.

Teng H. H., Dove P. M., and DeYoreo J. J. (2000) Kinetics of calcite growth: surface processes and relationships to macroscopic rate laws. *Geochim. Cosmochim. Acta* **64,** 2255–2266.

Teng H. H., Dove P. M., Orme C. A., and De Yoreo J. J. (1998) Thermodynamics of calcite growth: baseline for understanding biomineral formation. *Science* **282,** 724–727.

Tesoriero A. J. and Pankow J. F. (1996) Solid solution partitioning of Sr^{2+}, Ba^{2+} and Cd_{2+} to calcite. *Geochim. Cosmochim. Acta* **60** (*6*),1053–1063.

Thomas T. N., Land T. A., Casey W. H., and De Yoreo J. J. (2004) Emergence of supersteps on KH_2PO_4 crystal surfaces. *J. Cryst. Growth* **92**: 216103/1–4.

Wasylenki L. E., Dove P. M., and De Yoreo J. J. (in press) Calcite growth as a function of temperature in the presence of Mg^{2+}: A critical step toward robust calcite paleothermometry. *Geochim. Cosmochim. Acta.*

Watson E. B. (1996) Surface enrichment and trace-element uptaking during crystal growth. *Geochim. Cosmochim. Acta* **60,** 5013–5020.

Watson E. B. (2004) A conceptual model for near-surface kinetic controls on the trace-element and stable isotope composition of abiogenic calcite crystals. *Geochim. Cosmochim. Acta* **68,** 1473–1488.

Wilson D. S. (2003) Nanoscale effects of strontium on calcite growth: A baseline for understanding biomineralization. Master's thesis, Virginia Tech.